Drive torque actuation in active surge control of centrifugal compressors

Jan Tommy Gravdahl*†, Olav Egeland* and Svein Vatland‡

*Dept of Engineering Cybernetics
Norwegian U. of Science and Tech.,
N-7491 Trondheim,
Norway

†ABB Industri AS
Hasleveien 50
N-501 Oslo
Norway

‡ABB Corporate Research
Bergerveien 12
N-1375 Billingstad
Norway

Submitted to Automatica
Revised 4th January 2002

Abstract

A novel aproach to active surge control is presented for a centrifugal compressor driven by an electrical motor. The main idea of the paper is to use the *drive itself* for surge control. This eliminates the need for additional actuators, and has the potential of energy efficient operation. It is shown that previous unstable operating points to the left of the surge line can be made globally exponentially stable by using the rotational speed of the motor as control. It is then shown that the results still hold when the torque of the drive is considered to be the control input. The proposed method is simulated on a compressor model using an approximation of a real compression system.

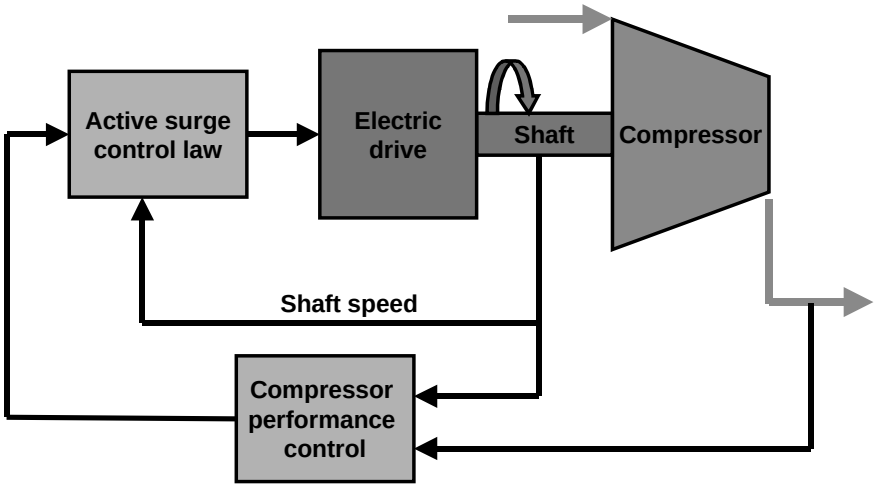

Figure 1: The compression system consists of a centrifugal compressor driven by an electrical motor.

1 Background

Surge is an unstable operation mode of centrifugal compressors which occurs when the operating point of the compressor is to the left of the surge line, which is the stability limit in the compressor map. Surge has been a major problem for designers and users of compressors since the invention of the turbocompressor. The phenomenon itself and the mechanism behind it is was recognized as early as 1924 by Stodola. Also, according to Whittle (1953) surge was a serious problem in designing centrifugal compressors for the first jet engines. One of the first attempts to model surge mathematically was made by Emmons, Pearson and Grant (1955), and a dynamic model suitable for control design was developed by Greitzer (1976). A general overview over surge phenomena can be found in Greitzer (1981) or in textbooks like Cumpsty (1989).

The surge phenomenon is manifested as oscillations of the mass flow, the pressure rise and the rotational speed of the compressor. Surge is highly undesired, and can cause severe damage to the machine. Traditionally, surge has been avoided using surge avoidance schemes. An example of such a scheme may be found in Staroselsky and Ladin (1979), and other methods may be found in Nisenfeld (1982) and Botros and Henderson (1994). Surge avoidance schemes use various techniques to keep the operating point of the compressor away from the surge line. Typically, a surge control line is drawn at a specified distance from the surge line, and the surge avoidance scheme ensures that the operating point does not cross this line. Usually a recycle line with a recycle valve is constructed around the compressor and used for actuation. This method works well, as has been proved by numerous installations. However, due to the presence of the surge margin, the method restricts the operating range of the machine, and achievable efficiency is limited.

Active surge control is fundamentally different to surge avoidance as unstable equilibria are sought to be stabilized instead of avoided. The motivation behind this is to overcome some of the shortcomings of surge avoidance. Active surge control of compressors was first introduced by Epstein, Williams and Greitzer (1989), and since then a number of theoretical and experimental results have been published. Different actuators have been used, and examples include recycle valves, bleed valves and throttle valves, gas injection and variable guide vanes. For an overview, consult de Jager (1995), Gravdahl and Egeland (1999b) or Willems and de Jager (1999).

In this study, which is on compressors with electrical drives, we propose to use the electrical drive as a means of active surge control, as depicted in Figure 1. The advantage of this is that the drive is already present, and no additional actuation device is required. This means that the compressor can be operated at a low flow without recycling, and there is a potential for reduced energy consumption of the compressor.

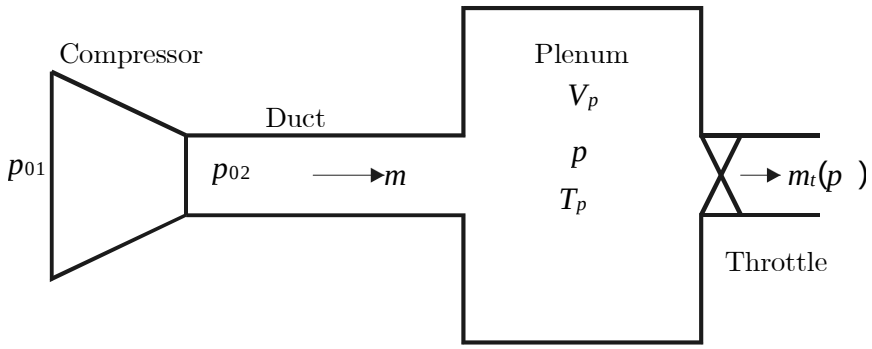

Figure 2: The compressor, plenum, throttle system of (Greitzer 1976)

2 Model

2.1 Dynamics

A classical result in the field of compressor surge modeling is the model of Greitzer (1976) who modelled a basic compression system consisting of a compressor, a plenum volume, a throttle valve and in-between ducting as shown in Figure 2. In order to study the drive torque as a control variable for surge control, we need a model that takes variable speed into account. In Fink, Cumpsty and Greitzer (1992), the model of Greitzer was further developed, and rotational speed was included as a state in the model. A similar model, which will be used in this paper, was derived in Gravdahl and Egeland (1999a) by calculating the mass balance of the plenum volume, integrating the one dimensional Euler equation (the momentum balance) over the length of the exit duct, and calculating the torque balance of the rotating shaft. The model is written

$$\dot{p} = \frac{a_{01}^2}{V_p}(m - m_t(p)) \tag{1a}$$

$$\dot{m} = \frac{A_1}{L_c}(\Psi_c(\omega, m)p_{01} - p) \tag{1b}$$

$$\dot{\omega} = \frac{1}{J}(\tau_d - \tau_c), \tag{1c}$$

where p is the plenum pressure, m is the compressor mass flow, ω is the rotational velocity, A_1 is the throughflow area, L_c is the duct length, V_p is the plenum volume, a_{01} is the sonic velocity at ambient conditions, $m_t(p)$ is the throttle flow, J is the sum of the inertia of the impeller, shaft and drive, τ_d is the drive torque, τ_c is the compressor load torque and $\Psi_c(m, \omega)$ is the compressor characteristic, which will be presented in detail in Section 2.2.

We will study stabilization and consider the dynamics around an equilibrium point. The equilibrium values are denoted by $(\cdot)_0$, while deviations from the equilibrium are denoted by $\widehat{(\cdot)}$. The deviations from the equilibrium are written

$$\hat{m} = m - m_0 \tag{2a}$$

$$\hat{p} = p - p_0 \tag{2b}$$

$$\hat{\omega} = \omega - \omega_0 \tag{2c}$$

$$\hat{m}_t = m_t - m_{t0} \tag{2d}$$

$$\widehat{\Psi}_c(\hat{\omega}, \hat{m}) = \Psi_c(\hat{\omega} + \omega_0, \hat{m} + m_0) - \Psi_{c0} \tag{2e}$$

where the equilibrium values must satisfy

$$m_0 = m_{t0}, \quad p_0 = \Psi_{c0}.$$

The model (1) is transformed into the new coordinates (2) and is then written

$$\dot{\hat{p}} = \frac{a_{01}^2}{V_p}(\hat{m} - \hat{m}_t) \tag{3a}$$

$$\dot{\hat{m}} = \frac{A_1}{L_c}\left(\widehat{\Psi}_c\left(\hat{\omega}, \hat{m}\right) p_{01} - \hat{p}_p\right), \tag{3b}$$

$$\dot{\hat{\omega}} = \frac{1}{J}\left(\widehat{\tau}_d - \widehat{\tau}_c\right). \tag{3c}$$

For controller design we will first assume that control variable is the angular velocity ω of the compressor shaft. In that case, the model is simplified to

$$\dot{\hat{p}} = \frac{a_{01}^2}{V_p}(\hat{m} - \hat{m}_t) \tag{4a}$$

$$\dot{\hat{m}} = \frac{A_1}{L_c}\left(\widehat{\Psi}_c\left(\hat{\omega}, \hat{m}\right) p_{01} - \hat{p}_p\right). \tag{4b}$$

Then, later, we will study the effect of the fact that the control variable is the electrical motor torque τ_d , while ω is controlled by an internal high gain loop.

2.2 Nonlinearities

Derivation of the compressor characteristic The compression process is modeled as an isentropic compression from p_{01} to p_{02} followed by an isobaric entropy increase. The change in stagnation enthalpy in the isentropic compression is denoted Δh_{0s}, while according to Ferguson (1963) the entropy increase is due to the shock loss Δh_{0i} related to incidence loss at the blade inlet and in the diffuser, and the fluid friction loss Δh_{0f}. The total increase Δh_{0t} of the stagnation enthalpy of the fluid contributed by the rotor is

$$\Delta h_{0t}(\omega, m) = \Delta h_{0s}(\omega, m) + \Delta h_{0i}(\omega, m) + \Delta h_{0f}(m).$$

The compressor characteristic is defined by

$$\Psi_c\left(\omega, m\right) = \frac{p_{02}}{p_{01}}.$$

Then, from the standard isentropic relations we get

$$\Psi_c\left(\omega, m\right) = \left(\frac{T_{0cs}}{T_{01}}\right)^{\frac{\kappa}{\kappa-1}} = \left(1 + \frac{\Delta h_{0s}}{c_p T_{01}}\right)^{\frac{\kappa}{\kappa-1}} \tag{5}$$

where T_{0cs} is the stagnation temperature that would result at the rotor outlet if the compression from p_{01} to $\Psi_c p_{01}$ had been isentropic, and

$$\Delta h_{0s}(\omega, m) = \Delta h_{0t}(\omega, m) - \Delta h_{0i}(\omega, m) - \Delta h_{0f}(m). \tag{6}$$

Following Ferguson (1963), we assume the following expressions for the changes in stagnation enthalpy:

$$\Delta h_{0t} = \mu r_2^2 \omega^2 \tag{7a}$$

$$\Delta h_{0i} = \frac{r_1^2}{2}(\omega - \alpha m)^2 \tag{7b}$$

$$\Delta h_{0f} = k_f m^2. \tag{7c}$$

It is emphasized that the controller design and stability analysis presented below will still be valid for more elaborate expressions for the changes in stagnation enthalpy. In fact, the results that are presented are also valid for numerical approximations of the compressor characteristic $\Psi_c\left(\omega, m\right)$.

Combining the (5), (6) and (7), the following expression is found for the compressor characteristic :

$$\Psi_c(\omega, m) = \left(1 + \frac{\mu r_2^2\omega^2 - \frac{r_1^2}{2}(\omega - \alpha m)^2 - k_f m^2}{c_p T_{01}}\right)^{\frac{\kappa}{\kappa-1}} \tag{8}$$

Note that this expression is also valid in the unstable region to the left of the surge line. Here r_1 is the impeller radius, r_2 is the rotor diameter, k_f is the fluid friction constant, T_{01} is the inlet stagnation temperature, c_p is the specific heat at constant pressure, c_v is the specific heat at constant volume and $\kappa = c_p/c_v$ is the ratio of specific heats. The constant α determines the point of zero incidence loss, which occurs for $\omega - \alpha m = 0$. The constant is given by

$$\alpha = \frac{\cot\beta_{1b}}{\rho_1 A_1 r_1} = \frac{\omega_{surge\_line}}{m_{surge\_line}},$$

where β_{1b} is the inlet blade outlet angle and ρ_1 is the density. The function

$$\mu = \sigma\left(1 - \frac{\cot\beta_{2b}}{\rho_1 A_1 r_1}\frac{m}{\omega}\right),$$

where β_{2b} is the rotor blade angle, accounts for rotor blades that are swept forwards or backwards. The function decreases with increasing mass flow for the usual backwards swept solution for blade design where $\beta_{2b} < 90^o$. The constant $\sigma = 1 - (n_{blades})^{-1}$ which is slightly less than unity, is the Stanitz slip factor, where n_{blades} is the number of blades.

Properties of the compressor characteristic Now some properties of the compressor characteristic that will be of use in the following analysis will be presented. From the expression (5) we find that the slope of the compressor characteristic $\Psi_c(\omega, m)$ with respect to the shaft velocity ω is given by

$$\frac{\partial\Psi_c}{\partial\omega} = \frac{\kappa}{\kappa-1}\left(\frac{T_{0cs}}{T_{01}}\right)^{\frac{1}{\kappa-1}}\frac{1}{c_p T_{01}}\frac{\partial h_{os}}{\partial\omega} = \frac{\rho_d}{RT_{01}}\frac{\partial h_{0s}}{\partial\omega} = k_\rho\frac{\partial h_{0s}}{\partial\omega}, \tag{9}$$

where

$$\rho_d = \left(\frac{T_{0cs}}{T_{01}}\right)^{\frac{1}{\kappa-1}}\rho_{01}$$

is the density that would result at the rotor outlet if the compression from p_{01} to $\Psi_c p_{01}$ had been isentropic, and

$$k_\rho = \frac{\rho_d}{RT_{01}}$$

is a constant. By using the fact that $2\mu r_2^2 > r_1^2$, combining the derivative of (6) with respect to ω with (9), it is found that

$$g_\omega \triangleq \frac{\partial\Psi_c}{\partial\omega} = k_d\left(2\mu r_2^2\omega - r_1^2(\omega - \alpha m)\right) > 0. \tag{10}$$

This agrees with the well-known phenomenon that in centrifugal compressors the pressure ratio always increases with increasing shaft speed due to the centrifugal forces on the fluid. In a similar derivation as above, it is found that the slope of the compressor characteristic Ψ_c with respect to the mass flow m is

$$\begin{aligned} g_m \triangleq \frac{\partial\Psi_c}{\partial m} &= \frac{\rho_d}{RT_{01}}\frac{\partial h_{0s}}{\partial m} = k_d\left(\frac{\partial h_{0t}}{\partial m} - \frac{\partial h_{0i}}{\partial m} - \frac{\partial h_{0f}}{\partial m}\right) \\ &= k_d\left(r_1^2\alpha(\omega - \alpha m) - 2k_f m\right). \end{aligned}$$

Define the surge line mass flow by

$$m_{sl}(\omega) \triangleq \frac{r_1^2\alpha}{r_1^2\alpha^2 + 2k_f}\omega.$$

Then $g_m < 0$ to the right of the surge line, that is for $m > m_{sl}$, and $g_m > 0$ to the left of the surge line, where $m < m_{sl}$.

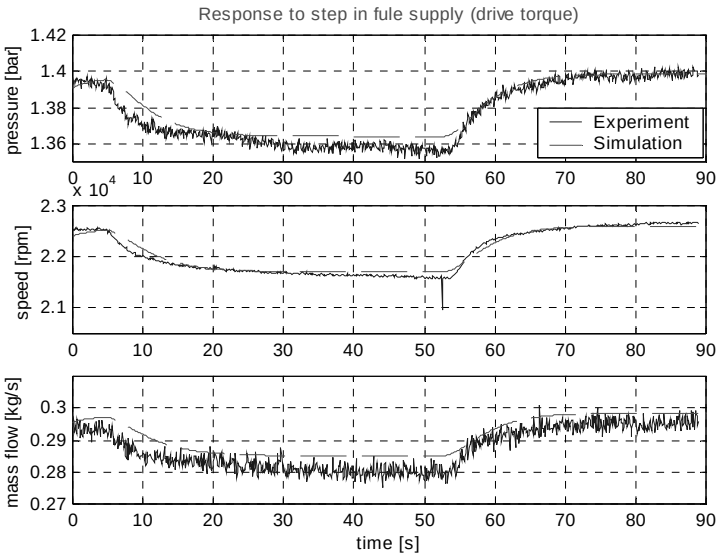

Figure 3: Changing the set point by changing the drive torque. The figure is taken from Gravdahl et al. (2000b).

Throttle mass flow The mass flow through the throttle is given by

$$m_t(p) = k_t\sqrt{p - p_{01}} = k_t\sqrt{p_{01}}\sqrt{\frac{p}{p_{01}} - 1}, \tag{11}$$

where the throttle parameter k_t is proportional to the valve opening.

Compressor torque As in Gravdahl and Egeland (1999a), the compressor torque τ_c can be calculated as

$$\tau_c(m, \omega) = \mu r_2^2 \omega m. \tag{12}$$

where r_2 is the impeller diameter.

2.3 Validation of the model

It is of great importance that the model (1) is accurate. Specifically, it is important that the effects of varying drive torque is captured as this is the basis for our control approach. Experimental results validating the model (1a)-(1c) with compressor map (8), throttle flow (11) and compressor torque (12) were presented in Gravdahl, Willems, de Jager and Egeland (2000a) and Gravdahl, Willems, de Jager and Egeland (2000b). Simulations of both normal (transient) operation (see Figure 3) and surge (see Figure 4) were compared to experiments with very good results. The experiments were done at The Energy Technology Laboratory at Eindhoven University of Technology where a gas turbine installation has been build around a BBC VTR 160L turbocharger. The installation is described in van Essen (1995).

3 Controller design

3.1 Surge control

The new feature of the proposed active surge control method is that we let the shaft velocity $\hat{\omega}$ be a function of the mass flow $\hat{m}$, thereby ensuring that the compressor can be operated to the left of the surge line without going into surge. We first assume that the shaft speed ω is our input control variable, and we will later consider the case that instead the drive torque τ_d is the control. The following theorem can now be stated:

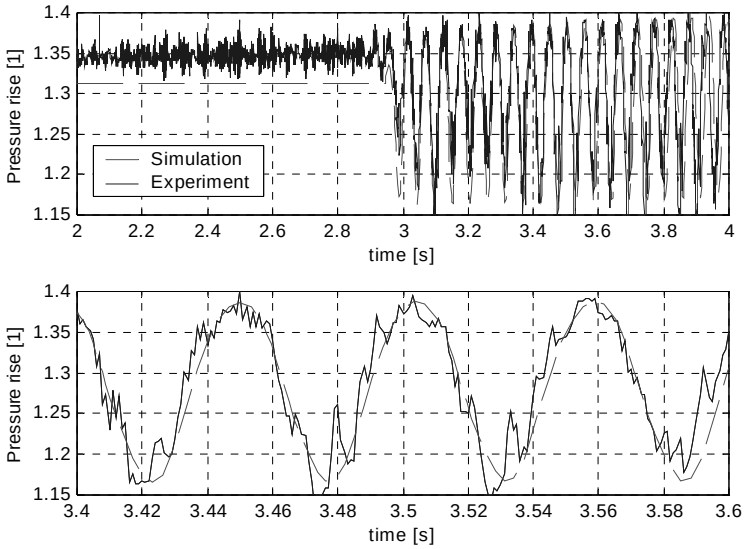

Figure 4: Surge oscillations. The results from the simulation are close to the experimental values. The figure is taken from Gravdahl et al. (2000b).

Theorem 1 *The control law*

$$\hat{\omega} = -c\hat{m}, \tag{13}$$

where the gain c is chosen according to

$$c > \frac{\partial \Psi_c / \partial m}{\partial \Psi_c / \partial \omega} = \frac{g_m}{g_\omega}$$

makes the origin of (4) globally exponentially stable.

Proof. Consider the Lyapunov function candidate

$$V = \frac{V_p}{2a_{01}^2}\hat{p}^2 + \frac{L}{2A}\hat{m}^2 > 0, \forall\,(\hat{m},\hat{p}) \neq (0,0) \tag{14}$$

The time derivative along the solutions of (4) is

$$\dot{V} = \frac{a_{01}^2}{V_p}\hat{p}\dot{\hat{p}} + \frac{L}{A}\hat{m}\dot{\hat{m}} = \hat{p}(\hat{m} - \hat{m}_t) + \hat{m}\left(\widehat{\Psi}_c p_{01} - \hat{p}\right)$$

This leads to the following expression for the time derivative:

$$\dot{V} = \dot{V}_1 + \dot{V}_2 = -\hat{p}\hat{m}_t\,(\hat{p}) + \hat{m}\widehat{\Psi}_c\,(\hat{m},\hat{\omega})\,p_{01} \tag{15}$$

The throttle, or load, is assumed to be passive in the sense that it consumes energy from the compressor, which implies

$$\dot{V}_1 = -\hat{p}\hat{m}_t\,(\hat{p}) < -k_p\hat{p}^2 < 0, \forall \hat{p} \neq 0 \tag{16}$$

for some $k_p > 0$, where k_p depends on the slope of the throttle characteristic. A plot of $\dot{V}_1$ is shown in Figure 5. In order to prove stability, we now have to show that $\dot{V}_2 = \hat{m}\widehat{\Psi}_c\,(\hat{m},\hat{\omega})\,p_{01} < 0$ when $\hat{\omega} = -c\hat{m}$.

As $\widehat{\Psi}_c\,(\hat{m},-c\hat{m})\Big|_{\hat{m}=0} = 0$, a sufficient condition for $\widehat{\Psi}_c\,(\hat{m},-c\hat{m})$ to be located in the 2nd and 4th quadrant in the $(\hat{m},\widehat{\Psi}_c)$-coordinate system is that $\widehat{\Psi}_c\,(\hat{m},\hat{\omega})\Big|_{\hat{\omega}=-c\hat{m}}$ is monotonically *decreasing*, that is

$$\frac{d\widehat{\Psi}_c\,(\hat{m},\hat{\omega})}{d\hat{m}} = \frac{\partial\widehat{\Psi}_c}{\partial\hat{m}} + \frac{\partial\widehat{\Psi}_c}{\partial\hat{\omega}}\frac{\partial\hat{\omega}}{\partial\hat{m}} = \frac{\partial\widehat{\Psi}_c}{\partial\hat{m}} - c\frac{\partial\widehat{\Psi}_c}{\partial\hat{\omega}} < 0 \tag{17}$$

where (13) has been used. The condition (17) is satisfied provided c is chosen according to

$$c > \frac{\partial \widehat{\Psi}_c \big/ \partial \hat{m}}{\partial \widehat{\Psi}_c \big/ \partial \hat{\omega}} = \frac{\partial \Psi_c / \partial m}{\partial \Psi_c / \partial \omega} = \frac{g_m}{g_\omega},$$

where the first equality follows from the coordinate shifts (2a), (2c) and (2e). $\widehat{\Psi}_c(\hat{m},\hat{\omega})\Big|_{\hat{\omega}=-c\hat{m}}$ is now monotonically decreasing and passing through the origin, that is located in the 2nd and 4th quadrants. Multiplying $\widehat{\Psi}_c(\hat{m},\hat{\omega})\Big|_{\hat{\omega}=-c\hat{m}}$ with $\hat{m}$, which belong to the 1st and 3rd quadrants, then results in

$$\dot{V}_2 = \hat{m}\widehat{\Psi}_c(\hat{m},-c\hat{m})\,p_{01} < 0, \forall \hat{m} \neq 0, \tag{18}$$

as is illustrated in Figure 6. Moreover, $\dot{V}_2$ can always be bounded from above as

$$\dot{V}_2 = \hat{m}\widehat{\Psi}_c(\hat{m},-c\hat{m})\,p_{01} < -k_m\hat{m}^2, \forall \hat{m} \neq 0. \tag{19}$$

for a constant $k_m > 0$. From (19) it follows that

$$\widehat{\Psi}_c(\hat{m},-c\hat{m})\,p_{01} < -k_m\hat{m},\ \hat{m} > 0. \tag{20}$$

As $\widehat{\Psi}_c(\hat{m},-c\hat{m})\,p_{01}$ is monotonically decreasing and passing through the origin, $\widehat{\Psi}_c(\hat{m},-c\hat{m})\,p_{01}$ is also bounded from above by the tangent through the origin, that is

$$\widehat{\Psi}_c(\hat{m},-c\hat{m})\,p_{01} < p_{01}\frac{d\widehat{\Psi}_c(\hat{m},-c\hat{m})}{d\hat{m}}\hat{m}.$$

By choosing

$$k_m = -p_{01}\frac{d\widehat{\Psi}_c(\hat{m},-c\hat{m})}{d\hat{m}}\bigg|_{\hat{m}=0}$$

(20) and (19) follows. A similar argument can be made for the case $\hat{m} < 0$. By (16), (19) and (14), we now have that

$$\dot{V} = \dot{V}_1 + \dot{V}_2 < -k_p\hat{p}^2 - k_m\hat{m}^2 < -kV, \forall\,(\hat{m},\hat{p}) \neq (0,0)\,,$$

where

$$k < \min\left\{\frac{k_p}{\frac{V_p}{2a_{01}^2}}, \frac{k_m}{\frac{L}{2A}}\right\}$$

and the result follows. ■

Remark 1. *It is seen from (13) that the gain c has a lower bound given by the ratio between the slope of the compressor characteristic* $\frac{\partial \Psi_c}{\partial m}$*, and the sensitivity of* Ψ_c *with respect to the shaft speed* ω*. This result is related to other results in active surge control for constant speed compressors, e.g.:*

- *When using the throttle valve for active surge control, Krstić, Fontaine, Kokotović and Paduano (1998) showed that the controller must have a gain that dominated the slope* $\frac{\partial \Psi_c}{\partial m}$ *of the compressor characteristic.*
- *When using a close coupled valve (CCV) to stabilize a centrifugal compressor, the control law gain must be greater than* $\frac{\partial \Psi_c}{\partial m}$*, as shown in Gravdahl and Egeland (1999a).*

Remark 2. *The CCV-approach, as introduced by Simon and Valavani (1991), aims at using the pressure drop over a valve to create a combined compressor and valve characteristic with negative slope in the equilibrium and thereby ensuring stability. It should be noted that the approach in this study achieves the same effect as the CCV approach without imposing an unwanted pressure drop in the compression system. The proposed controller ensures that in closed loop the compressor characteristic has a negative slope in the equilibrium*

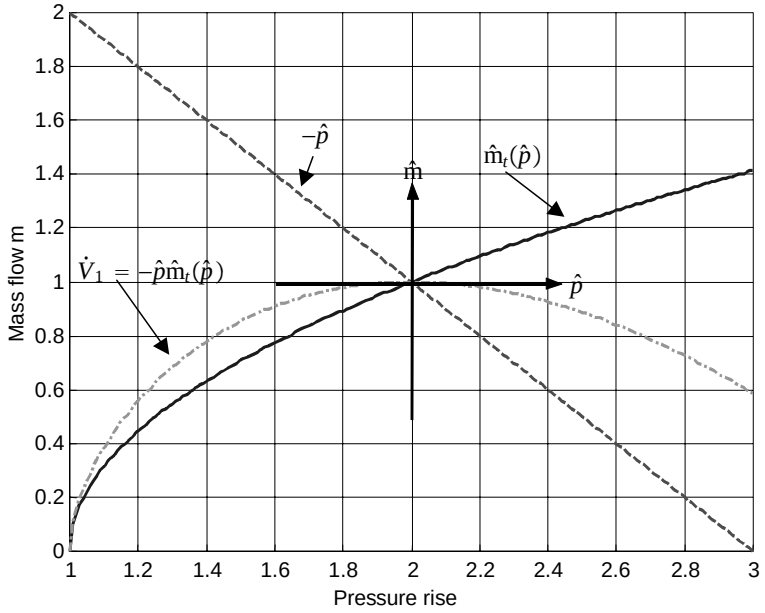

Figure 5: Illustration of the calculation of $\dot{V}_1$. The derivative of the LFC is shown relative to the $(\hat{p}, \hat{m})$-system.

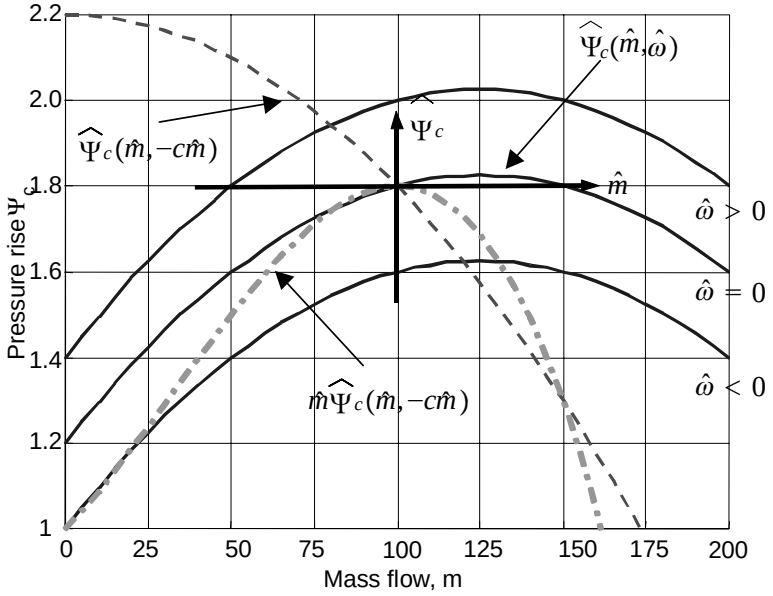

Figure 6: Illustration of the calculation of $\dot{V}_2$. The time derivative of the LFC is shown relative to the $\left(\hat{m}, \hat{\Psi}_c\right)$-system.

which can be seen from the plot of $\widehat{\Psi}_c(\hat{m}, -c\hat{m})$ *in Figure 6.*

We now take the shaft dynamics (3c) into consideration in order to investigate the effect on the stability properties of the system. Following the same procedure as in the proof of Theorem 1, the time derivative of the Lyapunov function candidate (14) along the trajectories of (4) is

$$\dot{V} < -k_p\hat{p}^2 - k_m\hat{m}^2 + \hat{m}\delta(t), \tag{21}$$

where

$$\delta(t) = \frac{A}{L}\widetilde{\Psi}_c(t),$$

and

$$\widetilde{\Psi}_c := \Psi_c(m,\omega) - \Psi_c(m,\omega_d) \tag{22}$$

is the error in the compressor pressure rise Ψ_c due to the shaft dynamics related to the convergence of ω to the desired value $\omega_d = \omega_0 - c\hat{m}$. It is seen from (21) that the system will converge towards a set $\mathcal{A}_1$, which will soon be defined, whenever

$$k_m|\hat{m}| > |\delta(t)|. \tag{23}$$

The set $\mathcal{A}_1$ can be found by using Young's inequality on the last term in (21) which gives

$$\hat{m}\delta(t) < \nu_1\hat{m}^2 + \frac{\delta^2(t)}{4\nu_1} < \nu_1\hat{m}^2 + \frac{\|\delta\|_\infty^2}{4\nu_1}, \quad \forall\nu_1 > 0, \tag{24}$$

where ν_1 is a constant. Consequently (21) can be written

$$\dot{V} < -k_p\hat{p}^2 - (k_m - \nu_1)\hat{m}^2 + \frac{\|\delta\|_\infty^2}{4\nu_1} = -W(\hat{x}) + \frac{\|\delta\|_\infty^2}{4\nu_1}, \tag{25}$$

where

$$\hat{x} = \begin{pmatrix} \hat{p} \\ \hat{m} \end{pmatrix}$$

and $W(\hat{x})$ is positive definite and radially unbounded provided the freely chosen ν_1 is selected such that

$$\nu_1 < k_m.$$

As $V(\hat{x})$ and $W(\hat{x})$ defined in (14) and (25) are quadratic, positive definite, radially unbounded and smooth there exist quadratic bounds such that

$$\begin{aligned} \beta_1\|\hat{x}\|^2 &\leq V(\hat{x}) \leq \beta_2\|\hat{x}\|^2 \\ \beta_3\|\hat{x}\|^2 &\leq W(\hat{x}), \end{aligned} \tag{26}$$

where β_1, β_2 and β_3 are positive constants. From (14) it is seen that $V = \hat{x}^T P\hat{x}$, where P is the positive definite matrix

$$P = \begin{pmatrix} \frac{V_p}{2a_{01}^2} & 0 \\ 0 & \frac{L}{2A} \end{pmatrix}.$$

Hence, β_1 and β_2 can be written $\beta_1 = \underline{\lambda}_P$ and $\beta_2 = \overline{\lambda}_P$, where $\overline{\lambda}_P = \max\left\{\frac{V_p}{2a_{01}^2}, \frac{L}{2A}\right\}$ and $\underline{\lambda}_P = \min\left\{\frac{V_p}{2a_{01}^2}, \frac{L}{2A}\right\}$ are the upper and lower eigenvalue of P. The constant $\beta_3 = \underline{\lambda}_Q$, where $\underline{\lambda}_Q = \min\{k_p, (k_m - \nu_1)\}$ is found from (25) in a similar manner. It now follows from (14), (25) and (26) that $\hat{x}(t)$ is globally uniformly bounded and converges to the compact set

$$\mathcal{A}_1 = \left\{\hat{x} : \|\hat{x}\| < \sqrt{\frac{\frac{\beta_2}{\beta_3}\frac{\|\delta\|_\infty^2}{4\nu_1}}{\beta_1}}\right\} = \left\{\hat{x} : \|\hat{x}\| < \frac{1}{2}\sqrt{\frac{\beta_2}{\beta_1\beta_3\nu_1}}\|\delta\|_\infty\right\}. \tag{27}$$

The compactness of $\mathcal{A}_1$ follows from the fact that the bounds in (26) are quadratic, as is discussed on p. 214 in Khalil (1996). The rate of convergence can be determined as follows. Consider the signal

$$s \stackrel{\triangle}{=} V(\hat{x})e^{\gamma t},$$

where γ is a constant. By using (25) and (26), the time derivative of s can be upper bounded as

$$\begin{aligned}
\frac{ds}{dt} &= \left(\dot{V} + \alpha V\right) e^{\gamma t} \\
&\leq \left(-W(\hat{x}) + \frac{\|\delta\|_\infty^2}{4\nu_1} + \alpha V\right) e^{\gamma t} \\
&\leq \left(-\beta_3 \|\hat{x}\|^2 + \gamma\beta_2 \|\hat{x}\|^2\right) e^{\gamma t} + \frac{\|\delta\|_\infty^2}{4\nu_1} e^{\gamma t}.
\end{aligned}$$

Now, chose γ as

$$\gamma \leq \frac{\beta_3}{\beta_2},$$

so that

$$\frac{ds}{dt} \leq \frac{\|\delta\|_\infty^2}{4\nu_1} e^{\gamma t}. \tag{28}$$

An upper bound on the state $\hat{x}$ is now found by integrating (28):

$$\begin{aligned}
\int_0^t \frac{ds}{dt'} dt' &\leq \int_0^t \frac{\|\delta\|_\infty^2}{4\nu_1} e^{\gamma t'} dt' \\
&\Downarrow \\
V(\hat{x}(t))e^{\gamma t} - V(\hat{x}(0)) &\leq \frac{\|\delta\|_\infty^2}{4\nu_1} \left(e^{\gamma t} - 1\right) \\
V(\hat{x}(t)) &\leq V(\hat{x}(0))e^{-\gamma t} + \frac{\|\delta\|_\infty^2}{4\nu_1}
\end{aligned} \tag{29}$$

By using (26) and (29) can be written

$$\begin{aligned}
\overline{\lambda}_P \|\hat{x}(t)\|^2 &\leq \overline{\lambda}_P \|\hat{x}(0)\|^2 e^{-\gamma t} + \frac{\|\delta\|_\infty^2}{4\nu_1} \\
\|\hat{x}(t)\| &\leq \|\hat{x}(0)\| e^{-\frac{\gamma}{2} t} + \frac{\|\delta\|_\infty}{2\sqrt{\nu_1 \overline{\lambda}_P}},
\end{aligned} \tag{30}$$

where the fact that $\sqrt{a^2 + b^2} \leq |a| + |b|$ has been used. By (30) it follows that $\hat{x}(t)$ converges to $\mathcal{A}_1$ with an exponential rate of convergence.

In the case that the desired speed ω_d is reached, we have the following useful result. Assume that there exists a non-negative monotonically decreasing function $\overline{\delta}(t)$ such that

$$|\delta(t)| < \overline{\delta}(t), \quad \forall t \geq 0 \tag{31}$$

and further assume $\omega \to \omega_d$ such that according to (22),

$$\lim_{t \to \infty} \delta(t) = 0. \tag{32}$$

It now follows from an analysis similar to the on page 77 in Krstić, Kanellakopoulos and Kokotović (1995) that in additional to being globally uniformly bounded, $\hat{x}(t)$ converges to the origin.

3.2 Velocity control

Let the electrical motor torque be generated by

$$\tau_d = \hat{\tau} + \tau_0$$

where

$$\tau_0 = \tau_{c0}$$

is the torque required in the equilibrium point, and

$$\hat{\tau} = K_1 (\omega_d - \omega)$$

is the feedback control law that is used to obtain the desired shaft speed

$$\omega_d = \omega_0 - c\hat{m}.$$

The resulting control law is

$$\tau_d = -K_1\hat{\omega} - K_2\hat{m} + \tau_0 \tag{33}$$

where the feedback gain for the mass flow is

$$K_2 = K_1 c.$$

In practical implementations we propose the use of integral action to generate the term τ_0. The integral term $-K_I \int_0^t \hat{\omega}(t')dt'$ is included in order to keep the compressor at the desired speed, and can be regarded as part of the performance control system, see Figure **??**. This gives the control law

$$\tau = -K_1\hat{\omega} - K_2\hat{m} - K_I \int_0^t \hat{\omega}(t')dt'. \tag{34}$$

By using the analysis presented in equations (21) to (23), it can be concluded that applying a drive torque according to (34) ensures that the states of the system (3) converges exponentially to a region around the origin.

3.3 Disturbances

Assume that the compression system is subject to disturbances $\delta_p(t)$ in pressure $\hat{p}$ and $\delta_m(t)$ in mass flow $\hat{m}$ so that the dynamics become

$$\dot{\hat{p}} = \frac{a_{01}^2}{V_p}(\hat{m} - \hat{m}_t) + \delta_p(t) \tag{35}$$

$$\dot{\hat{m}} = \frac{A_1}{L_c}\left(\widehat{\Psi}_c p_{01} - \hat{p}\right) + \delta_m(t). \tag{36}$$

Under the controller proposed in Theorem 1, the time derivative of the Lyapunov function candidate (14) along the trajectories of (35)-(36) becomes

$$\dot{V} < -k_p\hat{p}^2 - k_m\hat{m}^2 + \hat{p}\delta_p + \hat{m}\delta_m. \tag{37}$$

As the inclusion of disturbances lead to a LFC time derivative of the same structure as (21), an analysis similar to the one in equations (24) to (32) results in the following: The states of the system will be globally ultimately bounded and converge to a compact set

$$\mathcal{A}_2 = \left\{ \hat{x} : |\hat{x}| < \frac{1}{2}\sqrt{\frac{\beta_2}{\beta_1\beta_4}\left(\frac{\|\delta_p\|_\infty^2}{\nu_2} + \frac{\|\delta_m\|_\infty^2}{\nu_3}\right)} \right\}, \tag{38}$$

where the positive constant β_4 is found from the two first terms in (37), and ν_2 and ν_3 are constants introduced by applying Young's inequality to the last two terms in (37). The set $\mathcal{A}_2$ is found using the same technique leading to the set $\mathcal{A}_1$ in (27). The rate of convergence towards $\mathcal{A}_2$ will be exponential, and if the disturbances satisfy (31) and (32), the states will converge to the origin.

3.4 Torque actuation with disturbances

Including both shaft dynamics and disturbances allow us to combine the above calculations, resulting in an LFC time derivative

$$\dot{V} < -k_p\hat{p}^2 - k_m\hat{m}^2 + \hat{p}\delta_p + \hat{m}\delta_m + \hat{m}\delta(t), \tag{39}$$

from which it can be concluded that the controller (33) renders the states of the system (35)-(36) globally ultimately bounded. Exponential convergence to a compact set

$$\mathcal{A}_3 = \left\{ \hat{x} : |\hat{x}| < \frac{1}{2}\sqrt{\frac{\beta_2}{\beta_1\beta_5}\left(\frac{\|\delta\|_\infty^2}{4\nu_1} + \frac{\|\delta_p\|_\infty^2}{4\nu_2} + \frac{\|\delta_m\|_\infty^2}{4\nu_3}\right)} \right\}, \tag{40}$$

is ensured. The positive constant β_5 is found from the two first terms in (37) using the same technique as before.

4 Implementation issues

4.1 Introducing realistic disturbances

In order to simulate realistic situations, disturbances are introduced in the simulations of the system. Process disturbances in the form of mass flow fluctuations and measurement noise in the mass flow measurement will be considered. The disturbances are of three types:

Low/medium frequency process disturbances This is larger changes in mass flow due to operational changes for such events as start-up, shutdown, trip of an upstream or downstream compressor, rerouting of gas in a pipeline network etc. In actual compressor installations, such disturbances might cause the flow rate to increase/decrease by 10% over a 5-minute period. Also change in consumer demands might cause the flow rate to change in the area of 20%, but over a longer time period. The mass flow drop of 35% that drives the compressor into surge in the simulations in this study takes place at a time scale of 1 s, implemented here as a step which is filtered through a time constant with $T = 1$. The simulated disturbance is chosen to be a worst case version of real world disturbances.

High frequency process disturbances This is disturbances caused by such phenomena as e.g. slip relations between the different phases in a multiphase flow. The time series in the middle plot of figure 7 shows a scaled version of such a disturbance. The mass flow disturbance is taken from simulations of pipeline flow using a multi-phase simulator with a sampling interval of 1 s. Again, the disturbance is chosen according to a worst-case scenario.

Measurement noise The measurement noise is implemented in the simulations as band limited white noise with a power of 0.20 and a sampling interval of 0.010 s. This gives a measurement error in the range of ± 10 kg/s. The measured flow is in the order of 100 kg/s, which implies an measurement error of $\pm 10\%$. This is quite severe when compared to the mass flow measurement shown in the lower plot in Figure 3 which has a noise level of around $\pm 1.5\%$

Figure 7 shows the different disturbances that the compressor is experiencing in the simulations. The upper plot is the 35% drop in mass flow driving the compressor into surge. The middle plot is the process disturbances from the pipeline simulations, and the lower plot is the measurement noise.

4.2 Test rig considerations

As of now, plans are being made for a test rig in order to verify the methods in this study experimentally. Different test rig alternatives are being considered, and a number of issues are being studied in connection with this.

Of particular importance is that in a practical implementation the drive will have certain limitations. In the simulations presented in Section 5, these limitations are taken into account. This is implemented in

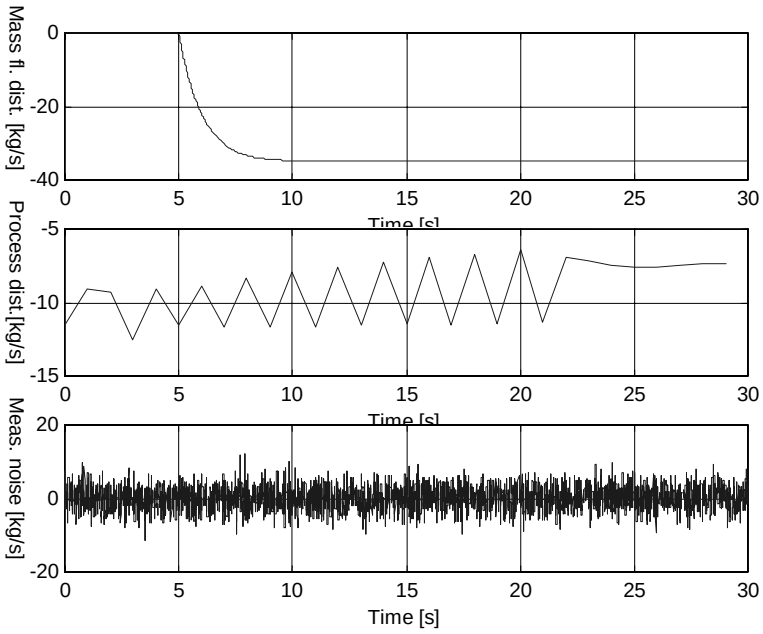

Figure 7: The different disturbances used in the simulations. From the top: Low/medium frequency process disturbances, High frequency process disturbances and Measurement noise.

the simulations by using various saturation elements. The limitations include maximum torque, maximum torque rate, maximum speed and maximum accelerations. Numerical values for the saturation limits are given in Appendix A.

When using the drive to actively control surge, it has been found through simulations that the mass flow measurement must be quite fast. In fact, simulations indicate that online measurement of mass flow with a time delay of no more that 50 ms is needed. This calls for a high speed mass flow measurement. On the other hand it is seen in Section 5 that measurement noise is handled well by the controller,

Other topics that have been considered, but which is outside the scope of this paper, include vibrations, thermal issues, limitations in the electrical supply grid, hysteresis due to stall and temporary loss of drive power.

5 Simulations

The compressor and electrical drive specified in Appendix A are used in the simulations. This could e.g. be a compression system for gas transport in pipelines.

5.1 Surge simulations

In this section results from simulations of the compressor system when it is driven into surge by a drop in mass flow is presented. The compressor is initially operating stable at $m \approx 100$ kg/s, when a drop in mass flow of 35% occurs resulting in deep surge. This mass flow drop is shown in the upper plot in Figure 7, and the compressor response to the disturbance is shown in Figure 8. A constant drive torque $\tau_d = 8000$ Nm is used. As the operating point crosses the surge line, the compressor undergoes deep surge with oscillations in mass flow, pressure rise and shaft speed. The surge frequency is about 1.6 Hz, which is typical for a compressor of this size. In Figure 9, the surge cycle is clearly visible on the compressor map. The reason for the higher rotational speed of the compressor during surge is that the drive torque is kept constant during simulation, and as can bee seen from (12) the compressor load torque is lower for this lower mass flow.

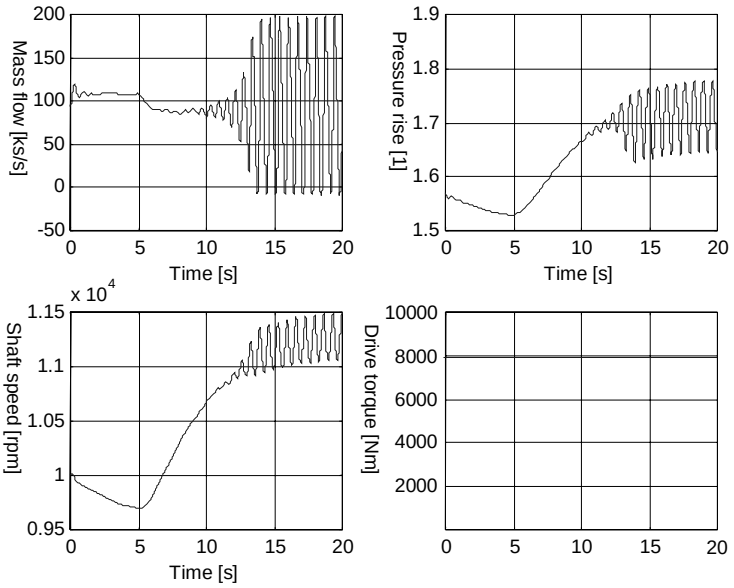

Figure 8: Compressor response due to 35% drop in mass flow. The system enters surge. The drive torque is kept constant.

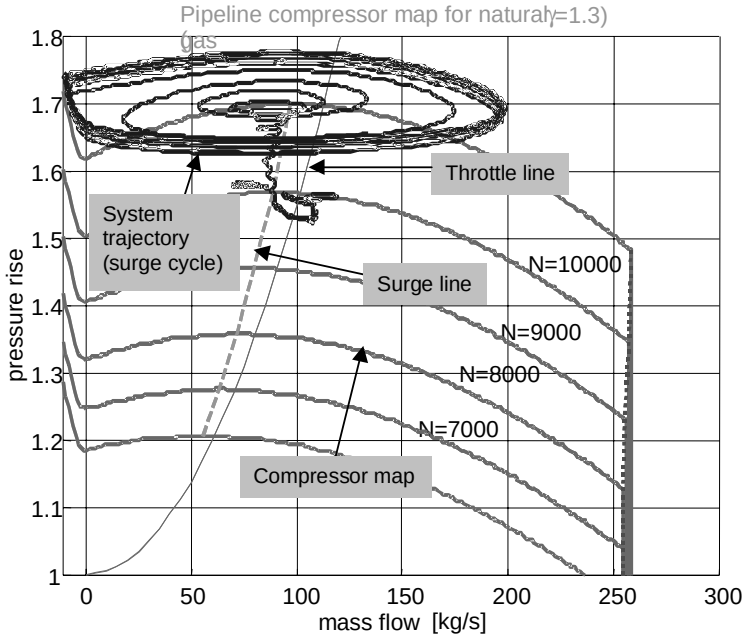

Figure 9: Surge simulation plotted together with the compressor map. The limit cycle is clearly visible.

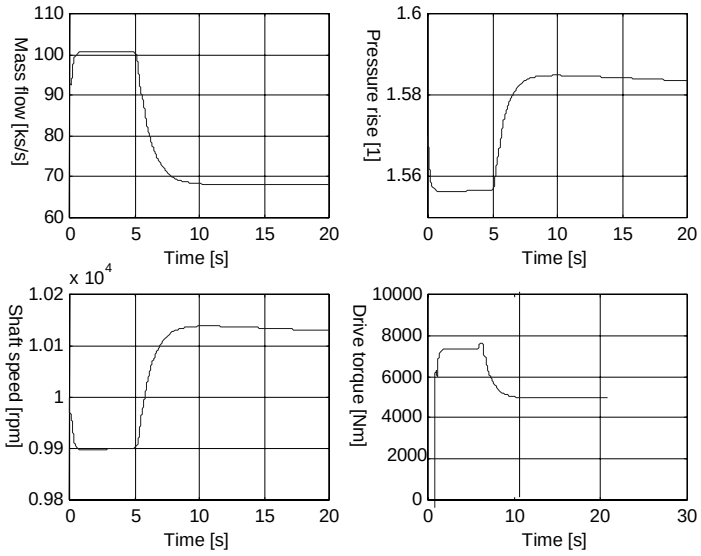

Figure 10: Stabilization of operating point left of the surge line using the control law (34).

5.2 Simulation of active surge stabilization

So far it has been demonstrated that the compressor becomes unstable when the operating point moves to far to the left of the surge margin. Simulations of the proposed active surge control approach will now be presented. The idea is to control the compressor speed with feedback from the mass flow so that the compressor can operate in a stable mode even to the left of the surge line and thereby avoiding the unstable operation demonstrated in the simulations above.

The controller is implemented with the input torque given by (34). The integral term $K_I \int_0^t \hat{\omega}(t')dt'$ is included in order to keep the compressor at the desired speed, and can be regarded as part of the performance control system. The following controller gains were used in all the simulations: $K_1 = 10000$, $K_2 = 500$ and $K_I = 10000$. Three simulation cases will be presented:

1. The compressor is driven over the surge line by a drop in mass flow.
2. Measurement noise is added.
3. Process disturbances is added.

5.2.1 Drop in mass flow

In this case the controller (34) is active at all times, and as the drop in mass flow is introduced at $t = 5$s, the compressor remains stable. This can bee seen in Figure 10, where the mass flow, pressure rise, shaft speed and drive torque are plotted as a function of time. As can be seen in Figure 11, the new stable operating point is located to the left of the surge line, illustrating the capability of the control system to achieve active surge control.

5.2.2 Surge control with measurement noise

In this case the high frequency measurement noise is taken into account. The noise is shown in the lower plot in Figure 7, and the resulting simulations are shown in Figure 12 and Figure 13. Due to the measurement noise, the drive torque τ_d, shown in the lower right subplot of Figure 12, is now quite noisy. However it is important to stress that the limitations of the drive, specified in Appendix A, is not exceeded.

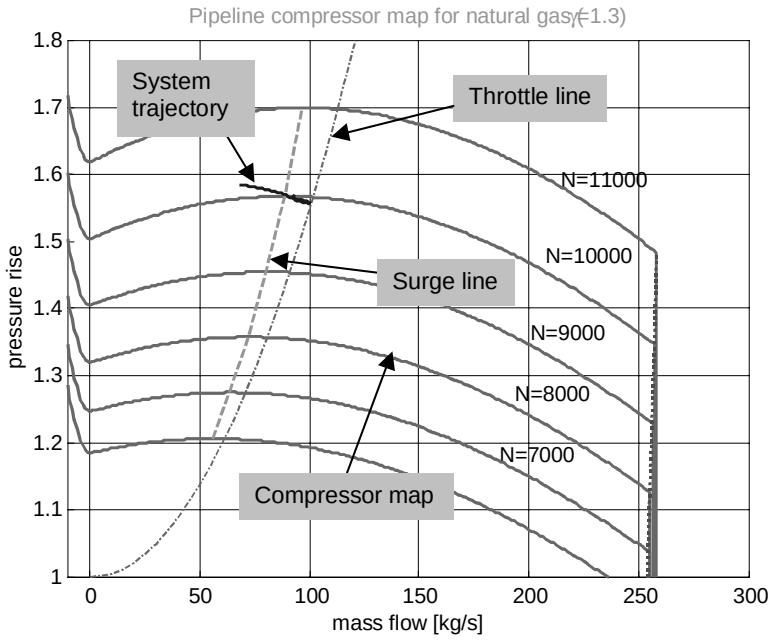

Figure 11: Same simulation as in Figure 10 plotted together with the compressor map. The system trajector crosses the surge line and reaches the stabilized operating point.

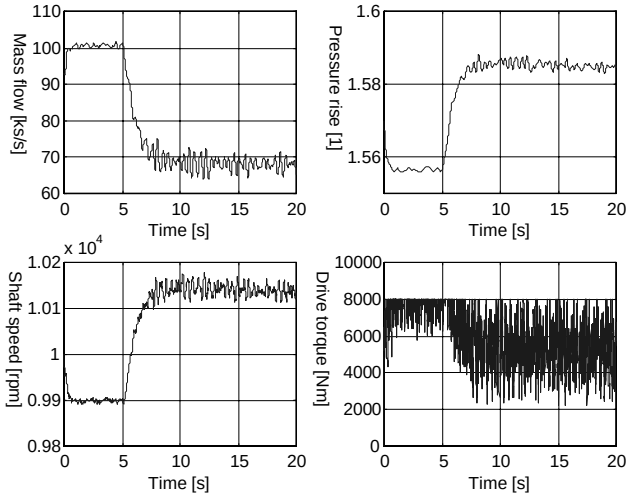

Figure 12: Same situation as in Figure 10, with the addition of measurement noise.

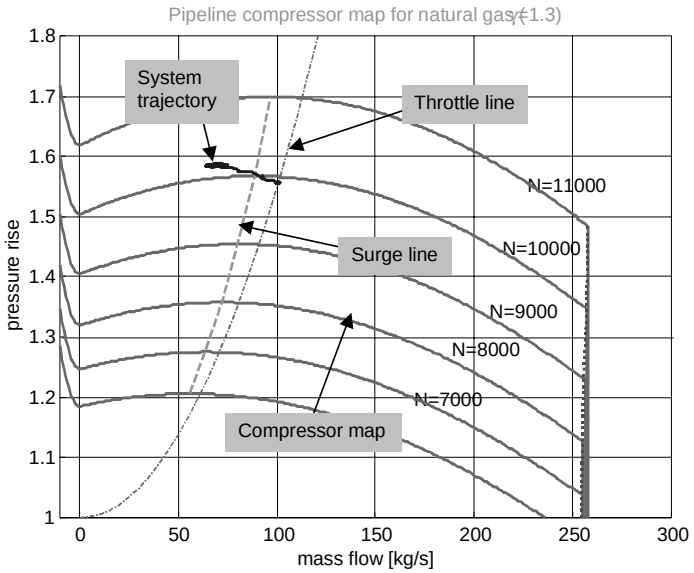

Figure 13: Same simulation as in Figure 13 plotted together with the compressor map.

5.2.3 Surge control with measurement noise and process disturbances.

In this case measurement noise, process disturbances are taken into account. The process disturbance is shown in the middle plot in Figure 7. As can bee seen from the plots in Figure 14 and Figure 15, the controller keep the compressor stable.

6 Conclusion

In this paper, we have developed a novel active surge controller for centrifugal compressors. By using the electrical drive as actuator and employing feedback from mass flow and rotational speed it has been shown that open loop unstable operating points in the area to the left of the surge line can be made globally exponentially stable. Exponential convergence is ensured in the presence of process disturbances and measurement noise. The results have been confirmed by simulations of a centrifugal pipeline compressor.

References

Botros, K. and Henderson, J.: 1994, Developments in centrifugal compressor surge control–a technology assessment, *Journal of turbomachinery* **116**, 240–249.

Cumpsty, N.: 1989, *Compressor Aerodynamics*, Longman.

de Jager, B.: 1995, Rotating stall and surge control : A survey, *Proceedings of the 35th Conference on Decision and Control*, New Orleans, LA, pp. 1857–1862.

Emmons, H., Pearson, C. and Grant, H.: 1955, Compressor surge and stall propagation, *Transactions of the ASME* **77**, 455–469.

Epstein, A., Williams, J. F. and Greitzer, E.: 1989, Active suppression of aerodynamic instabilities in turbomachines, *Journal of Propulsion and Power* **5**(2), 204–211.

Ferguson, T.: 1963, *The centrifugal compressor stage*, Butterworths, London.

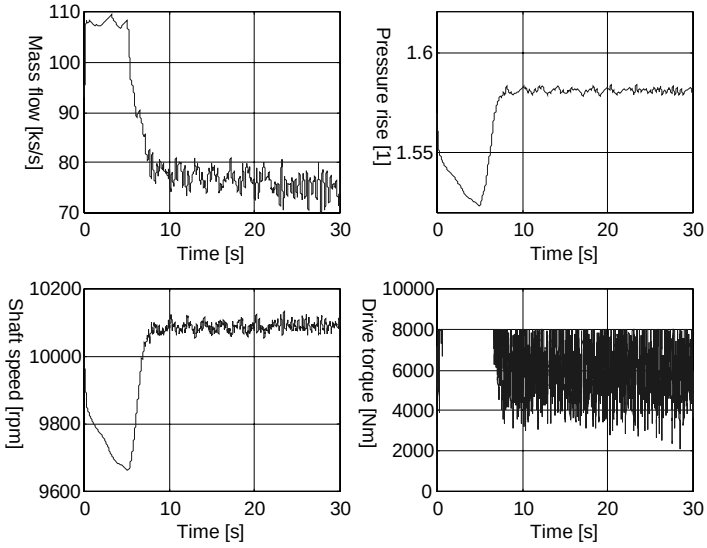

Figure 14: Same situation as in the ideal case, but now process disturbances and measurement noise is included.

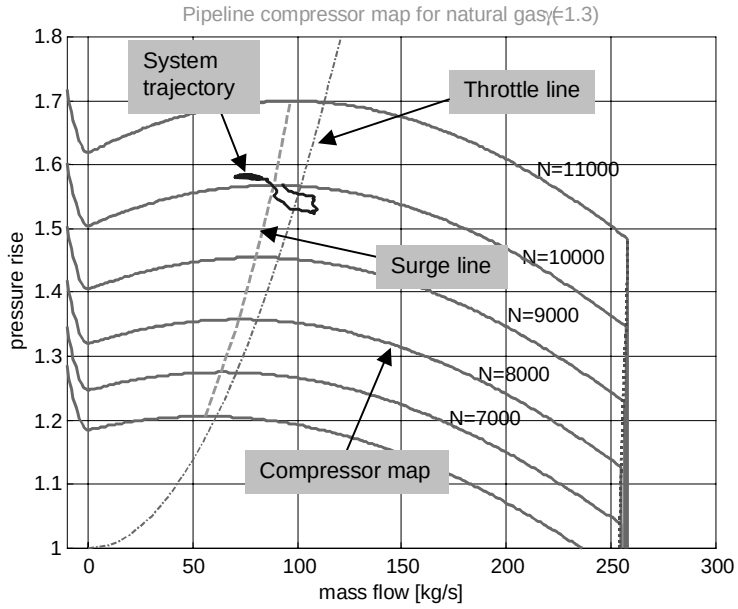

Figure 15: Same simulation as in Figure 14 plotted together with the compressor map.

Fink, D., Cumpsty, N. and Greitzer, E.: 1992, Surge dynamics in a free-spool centrifugal compressor system, *Journal of Turbomachinery* **114**, 321–332.

Gravdahl, J. and Egeland, O.: 1999a, Centrifugal compressor surge and speed control, *IEEE Transactions on Control Systems Technology* **7**(5).

Gravdahl, J. and Egeland, O.: 1999b, *Compressor surge and rotating stall: modeling and control*, Advances in Industrial Control, Springer-Verlag, London.

Gravdahl, J., Willems, F., de Jager, B. and Egeland, O.: 2000a, Modeling for surge control of centrifugal compressors: Comparison with experiment, *Proceedings of the 39th IEEE Conference on Decision and Control*, Sydney, Australia.

Gravdahl, J., Willems, F., de Jager, B. and Egeland, O.: 2000b, Modeling for surge control of centrifugal compressors: Experimental validation. Submitted to IEEE Transactions on control systems technology.

Greitzer, E.: 1976, Surge and Rotating stall in axial flow compressors, Part I: Theoretical compression system model, *Journal of Engineering for Power* **98**, 190–198.

Greitzer, E.: 1981, The stability of pumping systems – The 1980 Freeman scholar lecture, *Journal of Fluids Engineering* **103**, 193–242.

Khalil, H.: 1996, *Nonlinear systems*, 2nd edn, Prentice-Hall, Inc.

Krstić, M., Fontaine, D., Kokotović, P. and Paduano, J.: 1998, Usful nonlinearities and global stabilization of bifurcations in a model of jet engine surge and stall, *Transactions on automatic control* **43**(12), 1739–1745.

Krstić, M., Kanellakopoulos, I. and Kokotović, P.: 1995, *Nonlinear and Adaptive Control Design*, John Wiley & Sons Inc.

Nisenfeld, A.: 1982, *Centrifugal compressors: principles of operation and control*, Instrument society of America.

Simon, J. and Valavani, L.: 1991, A Lyapunov based nonlinear control scheme for stabilizing a basic compression system using a close-coupled control valve, *Proceedings of the 1991 American Control Conference*, pp. 2398–2406.

Staroselsky, N. and Ladin, L.: 1979, Improved surge control for centrifugal compressors, *Chemical engineering* pp. 175–184.

Stodola, A.: 1924, *Dampf und Gasturbinen*, Julius Springer, Berlin. Sechste auflage.

van Essen, H.: 1995, Design of a laboratory gas turbine installation, *Technical Report WOC-WET 95.012*, Eindhoven University of Technology.

Whittle, S.: 1953, *JET. The story of a Pioneer*, Frederick Muller Ltd, London.

Willems, F. and de Jager, B.: 1999, Modeling and control of compressor flow instabilities, *IEEE Control systems* **19**(5), 8–18.

A Single stage natural gas compressor

The main dimensions of a typical impeller of a single stage centrifugal compressor have been determined for use in the simulations. The compressor is compressing gas with properties $\kappa = 1.3$ and $c_p = 2064$ J/kgK. The design point is chosen as $m_d = 100$ kg/s, $p_d = 60$ bar, $T_d = 293$ K and $\pi_d = \frac{p_{02}}{p_{01}} = 1.5$. Relevant parameters for the compressor and an actual electrical drive used in the simulations are given in Table 1 and Table 2, respectively.

Outer diameter	$d_2 = 0.557$ m
Inlet diameter (hub)	$d_{h1} = 0.095$ m
Inlet diameter (shroud)	$d_{s1} = 0.210$ m
Blade height at shroud	$b_2 = 8$ mm
no. of blades	$Z = 22$
Blade inlet angle	$\beta_{1b} = 41°$
Moment of inertia	$I_c = 0.9$ kgm^2
Speed	$n = 10000$ rpm
Power consumption	$P_c = 7.5$ MW
Required torque	$\tau_c = 7100$ Nm

Table 1 Compressor specifications

Maximum torque	$\tau_{d,\max} = 8000$ Nm
Maximum torque rate	$\left.\frac{d\tau_d}{dt}\right\|_{\max} = 318320$ Nm/s
Moment of inertia	$I_d = 35$ kgm^2
Maximum speed	$N_{\max} = 12000$ rpm
Maximum acceleration	$\left.\frac{dN}{dt}\right\|_{\max} = 17.4$ 1/s^2

Table 2 Drive specifications